RESEARCH PAPER

Self-assembly of robotic micro- and nanoswimmers using magnetic nanoparticles

U. Kei Cheang · Min Jun Kim

Abstract Micro- and nanoscale robotic swimmers are very promising to significantly enhance the performance of particulate drug delivery by providing high accuracy at extremely small scales. Here, we introduce micro- and nanoswimmers fabricated using self-assembly of nanoparticles and control via magnetic fields. Nanoparticles self-align into parallel chains under magnetization. The swimmers exhibit flexibility under a rotating magnetic field resulting in chiral structures upon deformation, thereby having the prerequisite for non-reciprocal motion to move about at low Reynolds number. The swimmers are actuated wirelessly using an external rotating magnetic field supplied by approximate Helmholtz coils. By controlling the concentration of the suspended magnetic nanoparticles, the swimmers can be modulated into different sizes. Nanoscale swimmers are largely influenced by Brownian motion, as observed from their jerky trajectories.

Guest Editors: Leonardo Ricotti, Arianna Menciassi

This article is part of the topical collection on Nanotechnology in Biorobotic Systems

U. K. Cheang · M. J. Kim (✉)
Department of Mechanical Engineering & Mechanics,
Drexel University, Philadelphia, PA, USA
e-mail: mkim@coe.drexel.edu

The microswimmers, which are roughly three times larger, are less vulnerable to the effects from Brownian motion. In this paper, we demonstrate responsive directional control of micro- and nanoswimmers and compare their respective diffusivities and trajectories to characterize the implications of Brownian disturbance on the motions of small and large swimmers. We then performed a simulation using a kinematic model for the magnetic swimmers including the stochastic nature of Brownian motion.

Introduction

The prospect of micro- and nanorobotics to revolutionize many biomedical applications (Dogangil et al. 2008; Ferreira et al. 2004; Fusco et al. 2013a; Grady et al. 1990; Kim et al. Kim et al. 2013a; Liu et al. 2009; Martel et al. 2007; Mathieu et al. 2006; Zhang et al. 2005) have facilitated the interest to investigate controllable micro- and nanoscale devices capable of accessing small space at low Reynolds number (Abbott et al. 2009a; Avron et al. 2005; Najafi and Golestanian 2004; Ogrin et al. 2008; Yesin et al. 2005). Of particular interest to this work is drug delivery, which in itself is a topic with vast room for technological improvements along with many considerations and

challenges needed to be addressed. While it had been shown that particulate drug delivery systems offer many advantages for targeted delivery to tumors or organs (Clearfield 1996; Singh and Lillard 2009), various obstacles continue to hamper developments in this area (Tan et al. 2010); one such obstacle is target accuracy for drug accumulation (Bae and Park 2011). Magnetic particles controlled using a magnetic gradient have been explored to improve targeting capability (Dobson 2006; Sun et al. 2008), but this is not without limitations. Magnetic gradient force is relatively ineffective in such small scales (Abbott et al. 2009b; Vartholomeos et al. 2011) and the rapidly diminishing strength at long distances renders complications in direct control of particles (Mody et al. 2014). Micro- and nanoswimmers with active propulsion mechanisms can effectively move through small spaces and requires less applied magnetic field strength to do so (Abbott et al. 2009b). At micro- and nanoscales, locomotion must abide with the physics at low Reynolds number, which means that inertia is negligible. Following Purcell's work on non-reciprocal swimming (Purcell 1977), many strategies were developed for low Reynolds number locomotion by utilizing biologically inspired mechanisms such as the bacterium-like rotating chiral microswimmers (Cheang et al. 2010; Ghosh and Fischer 2009; Peyer et al. 2011; Temel and Yesilyurt 2011; Tottori et al. 2012) and the sperm-like flexible microswimmers (Dreyfus et al. 2005; Gao et al. 2012). While chirality and flexibility are the field's standards for designing microswimmers, other work such as the electrically controlled micro-biorobots (Steager et al. 2011), magnetically steered ciliate protozoa (Kim et al. 2010), the 3-bead achiral microswimmers (Cheang et al. 2014a, b), chemically driven propellers (Gao et al. 2013; Manesh et al. 2010; Solovev et al. 2009), bi-flagellated micro objects (Mori et al. 2010), and optically deformed 3-bead swimmers (Leoni et al. 2009) demonstrated effective low Reynolds number propulsion.

Existing microswimmers are generally constrained by high cost, complex fabrication, and/or application-limiting designs. Helical and flexible body swimmers are very effective swimmers in bulk fluid, but current micro- and nanofabrication methods are costly, complex, and size limiting. It should be noted that advances in nanofabrication have and will significantly reduce fabrication complicity and size limitations, such as the case with the Nanoscribe system. Biological swimmers,

such as the bacteria-powered microrobots (Steager et al. 2011) and the artificially magnetotactic *Tetrahymena pyriformis* (Kim et al. 2010), on the other hand are easy to fabricate due to massive cell culturing, but are not suited for drug delivery as well as other in vivo applications. Chemical propellers are fast swimmers, but the biocompatibility issues of their chemical byproducts may lead to complications with nearby tissues and cells. Alas, the pursuit for an effective propulsion system does not necessarily means the pursuit of an effective drug delivery system. Although to be fair, the aforementioned swimmers are useful in their own rights for their capability to navigate and manipulate at microscale which can be advantageous for a number of applications (Dogangil et al. 2008; Fusco et al. 2013b; Kim et al. 2013b; Magdanz et al. 2013; Solovev et al. 2012; Tottori et al. 2012; Xi et al. 2013), and none of them claimed a specificity for drug delivery. In particular, the nanovoyager (Venugopalan et al. 2014) demonstrated in biological environments, such as blood, served as a great example of the possibility to use microrobots for biomedical applications. Keeping in line with the considerable advantages of using nanoparticles for drug delivery, we examine the scalable nanoscale assembly of magnetic nanoparticles (MNPs) to create micro- and nanoswimmers. The MNP swimmers can be actuated via rotating magnetic fields, and convert rotation motion into translation motion. A similar recent work has explored the use of carbon-coated iron oxide to create chiral nanopropellers (Vach et al. 2013). In contrast, our MNP uses purely magnetic force for assembly resulting in high-aspect-ratio flexible filament and we believe the simple self-assembly method, without a carbon coating, will allow for more flexibility for synthesis of particles and surface functionalization. Furthermore, the use of MNPs is appropriately fitting to the nanoparticulate drug delivery paradigm allowing these MNP swimmers to share the same advantages including but not limited to tissue penetrability, high carrier capacity, and functionalizable structure (Basar-kar and Singh 2007; Gelperina et al. 2005).

Materials and methods

Fabrication using nanoscale magnetic assembly

The MNP swimmers can be fabricated using magnetic self-assembly of nanoparticles; in this

work, we have used 50–100 nm nanoparticles (Iron(II, III) oxide 98+ %, Sigma-Aldrich 637106). The magnetic properties of the nanoparticles, including saturation magnetization, coercivity, remanent magnetization, and hysteresis loop, have been thoroughly investigated by Bajpai et al. (2013). Under an external magnetic field, the MNPs will magnetize and form chains that are flexible under time-varying magnetic fields (Biswal and Gast 2004; Cēbers and Javaitis 2004; Vuppu et al. 2003). The concentration of MNPs should be moderated in order to avoid uncontrollable aggregations; instead, controlling the time in which the MNPs are exposed to the magnetic field at the desired concentration can give us better control over how the particles assemble into various sizes of swimmers. In our procedure, we fine-tuned the magnetic field strength, magnetization time, and particle concentration through trial and error. The stages of the self-assembly fabrication are as following: (1) Dilute MNPs to 0.1 mg/ml using diH$_2$O; (2) magnetize them using a 5.06 mT magnetic field in the order of 10 s to form single chains with nanoscale widths, constituting as nanoswimmers; (3) prolong exposure to the magnetic field on the order of minutes leads to chain-to-chain aggregations to form chain bundles with microscale widths, constituting as microswimmers. Chain-to-chain aggregation phenomena similar to stage 3 of our fabrication process had been previously investigated (Fang et al. 2007; Ytreberg and McKay 2000). Figure 1a–c illustrates the fabrication process using magnetic self-assembly. We used image processing to calculate the size of the micro- and nanoswimmers (Fig. 1d).

Filament deformation and swimming motion

The interconnected MNPs of the swimmers experience stretching and bending due to hydrodynamic and magnetic forces. Under a high frequency rotating magnetic field, the hydrodynamic forces will be greater, resulting in greater deformation; vice versa for low frequency rotation. The resulting deformations allow the near-rod-like MNP chains to become chiral structures, which can produce propulsion when rotated. The deformation can be modeled using Hooke's law; the stretching free energy and bending free energy are
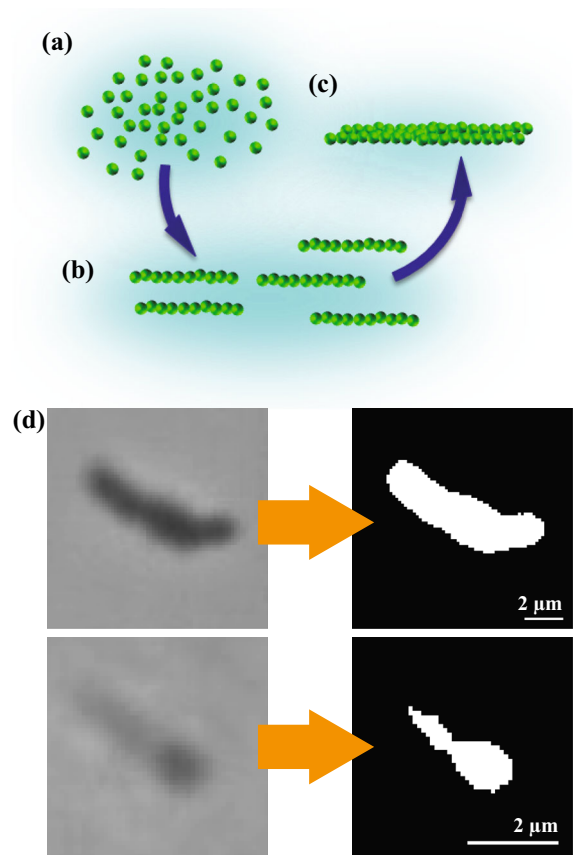
Fig. 1 Magnetic self-assembly in three stages to create micro- and nanoswimmers: **a** MNPs suspended in fluid. **b** MNPs forming nanoswimmers in the form of chains. **c** Chain aggregation forming microswimmers. **d** Tracking of a microswimmer using image processing to compute the size of the micro- and nanoswimmers

$$H^{S} = \frac{1}{2}k \sum_{i=2}^{N} (l_i - l_0)^2,$$

and

$$H^{S} = \frac{1}{2}A \sum_{0}^{L} ds \left(\frac{d\hat{t}}{ds}\right)^2,$$

respectively, where $l_i - l_0$ is the difference between the deformed and undeformed states, N is the number of beads, k is the spring constant, L is the length of the filament, s is the arc length along L, $\hat{t}$ is the unit tangent at s, and A is the bending stiffness (Gauger and Stark 2006). The dipole interaction between the beads contributes to the deformation. The dipole interaction energy between i-th and j-th beads is given as

$$H^{\mathrm{D}} = \frac{4\pi a^6}{9\mu_0}(\chi \boldsymbol{B})^2, \sum_{i,j=1}^{N} \frac{1 - 3(\hat{\boldsymbol{p}} \cdot \hat{\boldsymbol{r}}_{ij})}{r_{ij}^3}, \;\; i \neq j,$$

where μ_0 is the permeability of free space, is the magnetic susceptibility, $\boldsymbol{B}$ is the external field, $\boldsymbol{p}$ is the magnetic moment of the beads, $\boldsymbol{r}$ is their relative position (Gauger and Stark 2006).

The deformations of the MNP chains create the necessary chiral structures for low Reynolds number swimming. However, the rotation axis of the swimmer is the key to determine whether the swimmers will swim forward or not (Cheang et al. 2014b). This concept have been discussed in various work with magnetic swimmers, and the motions exhibited as a result of changing rotation axes have been called mode of motions (Cheang et al. 2014a), tumbling and precession (Ghosh et al. 2012, 2013a), and wobbling (Tottori et al. 2012). To change the rotating axis, we manipulated the rotating frequency and the applied field strength; in other words, we control the swimmers using the ratio of these two control parameters (Hz/mT). For the case with our MNP swimmers, the values for the ratio to achieve stable swimming ranges from 6.299 to 7.998 Hz/mT. The ranges of values were similar between the micro- and nanoswimmer due to the same MNPs used for both types of swimmers. For values greater than 7.998 Hz/mT, the swimmers experienced unsteady rotation, meaning that the rotation of the swimmer cannot follow the rotation of the magnetic field; this is also similar to the concept known as the step-out frequency (Cheang et al. 2014b; Tabak et al. 2011).

Magnetic control system

The control system used to generate the necessary rotating magnetic field to actuate the microswimmers consists of three pairs of electromagnetic coils arranged in an approximate Helmholtz configuration (Fig. 2), three programmable power supplies (Kepco BOP 20-5M), a NI data acquisition (DAQ) controller (PCI-6259 and BNC-2110), a workstation computer, an inverted microscope (Leica DM IRB), and a high speed camera (Fastcam SA3). The components are shown in Fig. 2c. The coil system is designed to exert torque on the microswimmers without introducing translational force; this is done so by applying a nearly uniform magnetic field rather than a gradient field through the approximate Helmholtz configuration. The six coils in the 3D approximate Helmholtz system are identical and are made up of 600 turns of copper wire (awg 25) bonded using epoxy. The inner and outer diameter of the coils are 4 and 6.55 cm, respectively, with coil thickness of 1.23 cm. Unlike a normal Helmholtz configuration, the distance between the coils is equal to the outer diameter of the coils.

Computer simulation and direct measurements from a tesla meter were used to model the magnetic field generated from the 3D coil system. With 1 Amp of current passing through two pairs of coils, the simulation result yielded a value of 5.06 mT at the center of the field, which matches the experimentally measured value of approximately 5 mT. We also investigated the field profile and demonstrated the ability of the coil system to generate a nearly uniform magnetic field at the center region approximately within a 2 mm diameter, which is indicated by the small circle at the center of the surface plot Fig. 2b. The profile of the magnetic flux density within the 2 mm region further indicates near uniformity (Fig. 2b). The size of this region approximately matches the size of the area where experiments take place. Given the size of the microswimmers being tested, the 2 mm region provides sufficient space needed for experimentation.

The magnetic field strength (mT), rotational direction of the magnetic bead (clockwise or counterclockwise), and rotational frequency (Hz) of the field generated by the coils can be controlled through LabVIEW. The effective magnetic field ($\mathbf{B}$) is the vector resultant of the x-, y-, and z-components. To create a rotation, there must be at least two pairs of electromagnetic coils; for example, one pair in the y direction and one pair in the z direction create a rotating field in the yz-plane. The two pairs generate sinusoidal outputs with 90° phase lag. Using xy-planar control, the resultant field can be expressed as

$$\mathbf{B} = \begin{bmatrix} -B_{\mathrm{s}}\cos(\theta) + B_{\mathrm{r}}\sin(\theta)\cos(\omega t) \\ B_{\mathrm{s}}\sin(\theta) + B_{\mathrm{r}}\cos(\theta)\cos(\omega t) \\ B_{\mathrm{r}}\sin(\omega t) \end{bmatrix}, \quad (1)$$

where B_r is the maximum amplitudes of the rotating magnetic field, B_s is the magnitude of the static magnetic field, ω is the rotational frequency of the
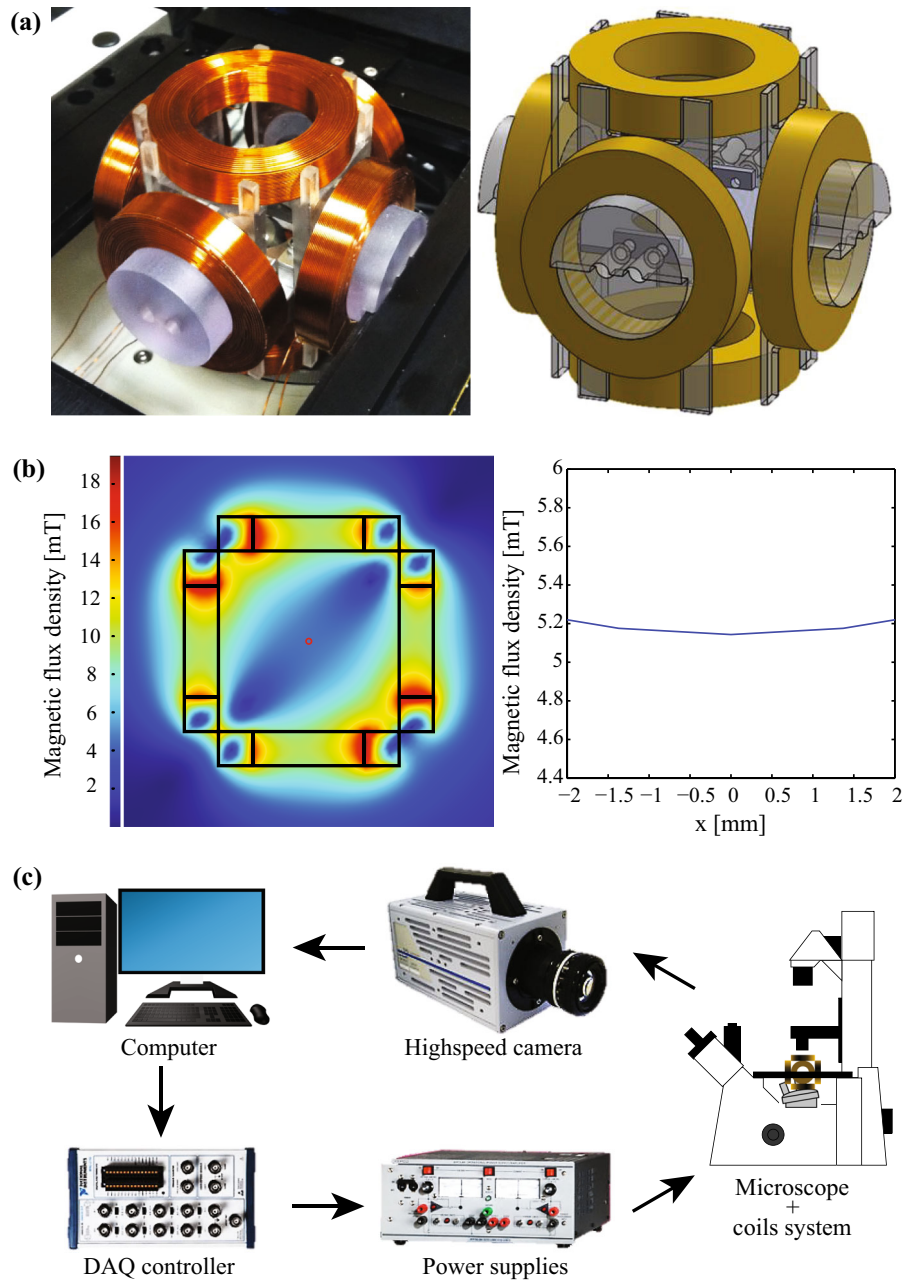
Fig. 2 The approximate Helmholtz configuration consists of three pairs of electromagnetic coils. **a** A photograph and CAD of the coil system. **b** COMSOL simulation showing a surface plot (*left*) of the magnetic field and the near uniform profile of the 2 mm region (*right*). **c** The components of the magnetic control system

field, θ is the direction of rotation, and t is time. Equation (1) rotates the plane of the rotating field and the perpendicular static field synchronously with θ. The perpendicular vector to the plane of the rotating field can be expressed as

$$\mathbf{n} = \begin{bmatrix} -\cos(\theta) & \sin(\theta) & 0 \end{bmatrix}^{T} \tag{2}$$

which also describes the swimming direction and the direction of the static field. A schematic for the model is shown in Fig. 3a.

Diffusivity

The diffusivity of the microswimmers is dependent on their perspective sizes. The theoretical diffusion coefficient can be computed using the Stokes–Einstein equation

$$D = \frac{k_B T}{f}, \tag{3}$$

where k_B is the Boltzmann constant, T is the temperature which is set at 297 K (room temperature), and f is the friction coefficient which accounts for size and shape of the object. The sizes of the swimmers were approximated using image processing (Fig. 1d). The nanoswimmers we've observed are roughly 2.78 μm in length and 0.90 nm in width, and the microswimmers are about 9.09 μm in length and 2.50 um in width. Using a rod-shaped model to approximate the drag on swimmers, the friction coefficient can be expressed as

$$f = \frac{3\pi\eta L}{\ln(L/d) + \gamma}, \tag{4}$$

where L and d are the length and diameter of the rod respectively, η is dynamic viscosity, and $\gamma = 0.312 + 0.565d/L - 0.1(d/L)^2$ is the end effect term (Cheong and Grier 2010; Ortega and de la Torre 2003). As a result, the diffusion coefficients D for microswimmers and nanoswimmers are 0.0944 and 0.2841 μm²/s, respectively. The diffusion coefficient for the nanoswimmers is roughly 3 times greater than that of the microswimmers; therefore, the nanoswimmers will be subjected to a stronger influence from Brownian motion.
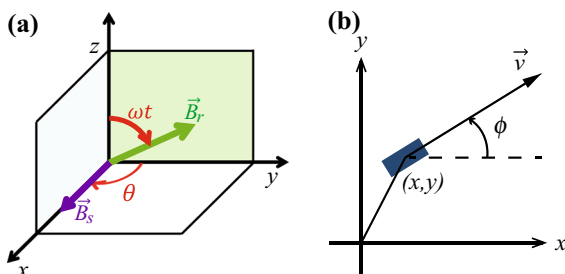
Fig. 3 Schematic for **a** the magnetic control system and **b** the kinematic models

Kinematic modeling

The kinematics of the MNP swimmers can be modeled as

$$\begin{aligned}
\dot{x}(t) &= v_1(\omega(t)) + b(t) \\
\dot{y}(t) &= v_2(\omega(t)) + b(t), \\
\dot{\phi}(t) &= \dot{\theta}(t),
\end{aligned} \tag{5}$$

where $v(\omega(t)) = [v_1(\omega(t)) \quad v_2(\omega(t))]^T = [\hat{a}\omega(t)\cos\phi(t)\,\hat{a}\omega(t)\sin\phi(t)]^T$, $\hat{a}$ can be approximate as the ratio between the average swimming speed v and rotation frequency ω, $b(t)$ represents random disturbances and noise, $\dot{\theta}$ is the input magnetic field's turning rate, and $\dot{\phi}$ is the rate of change of the heading angle. Here, we consider $b(t)$ as Brownian noise in the motion of the swimmers. Brownian is a constantly changing variable, they must be modeled stochastically. The orientation of the swimmers is directly controlled by the applied magnetics which overwhelms any effects from rotational diffusion, therefore, the random changes in orientation is ignored. Hence

$$b(t) = r_D(t) = P\sqrt{2Dt}, \tag{6}$$

where r_D is the displacement due to diffusion and P is a normally distributed pseudorandom numbers. A schematic for the model is shown in Fig. 3b.

Tracking algorithm

A MATLAB tracking algorithm was developed for post-processing analysis of the swimmers' motions. Raw data from experiments are video files (or sequence of images) taken at pre-set frame rates. The tracking algorithm performs image processing on the individual frames of the videos. The analysis involved four main steps: image binarization using grayscale thresholding, final structure definition, size thresholding, and calculation of geometrical centroid. In image binarization, the borders of the microswimmer were defined by setting a threshold defining a grayscale cutoff value and each individual frame was converted into a binary black/white image. After the structure edges were defined, the interior of the swimmer was filled using an additional algorithm. To remove unwanted objects such as debris or out-of-focus particles, size thresholding was used to filter out

objects bigger and smaller than the swimmer. The size of the objects was defined as the number of pixel they occupied. At this stage, the only remaining object should be the swimmer. After a binary image defining only the swimmer was obtained, the geometrical centroid (x,y) was calculated. The same four steps were then performed on sequential frames. The distance between the centroids of the consecutive frames was calculated based on the pixel-to-pixel distance, which was then converted to the displacement of the swimmer during the time interval.

Results and discussion

Manual control of micro- and nanoswimmers

To prepare for experiments, the micro- and nanoswimmers were resuspend in NaCl solution and then transferred to a polydimethylsiloxane (PDMS) chamber, which is 3 mm in diameter and 2 mm in height. The NaCl solution used during experiments helps matching the density of the swimmers and the fluid, which helps minimized sedimentation. This allows us to make sure the swimmers are swimming in bulk fluid rather than relying on surface interaction for locomotion. The NaCl solution also contributes to the aggregation of the MNPs, thereby, helps to preserve the structures of the swimmers (Elimelech et al. 1998). The chamber was sealed to prevent evaporation and minimize flow. The chamber was then placed inside the electromagnetic coil system for experiments. The range of magnetic fields used in the experiment is in the order of 1 mT.

During experiments, there are two ways to know that the swimmer is far from the boundary. First, during control of the microscope we always keep the focal plane at least 20 μm from the boundary. This may not be far enough to completely rule out the hydrodynamic interactions of 10 μm swimmers have with the walls. Second, the dynamics of the swimmers make it quite obvious when boundary effects become important: a rotor using the surface to move "rolls" along the surface and hence moves in a direction perpendicular to its rotation axis; in contrast, a swimmer in bulk fluid moves in a direction along the rotation axis.

Using the magnetic control system, we demonstrated steering control of both micro- and nanoswimmers. We obtained the nanoswimmers from stage 2 of the fabrication process. Figure 4 shows the trajectory of a representative example of a nanoswimmer. The nanoswimmer was traveling with a speed of 0.4912 μm/s under a 10 Hz rotation and responsive to the steering input. However, the movement of the nanoswimmer is influenced by Brownian motion, which is evident from the jerky trajectory. This kind of effect from Brownian motion is expected at the nanoscale. In contrast, the microswimmers obtained in stage 3 of the fabrication process have a much smoother trajectories, indicating a lesser influence by Brownian motion. A representative case of a microswimmer is shown in Fig. 5. To demonstrate the controllability, we manually steered the microswimmer to travel in a predefined path "DU". In Fig. 3, the "DU" path is shown as the dashed lines and the actual trajectory of the microswimmer is shown as the white solid line. The microswimmer traveled with a speed of 3.6655 μm/s under a 10 Hz rotation. The discrepancy between the trajectory and predefined path is due to the user's dexterity during manual control.

Measuring diffusivity

We further investigate the diffusion coefficient of the micro- and nanoswimmers without applying an external magnetic field; this means the swimmers are not exposed to external force with the exception of Brownian motion. To observe the diffusive motion of the swimmers, we used a tracking algorithm and computed the mean squared displacement (MSD) using this equation:
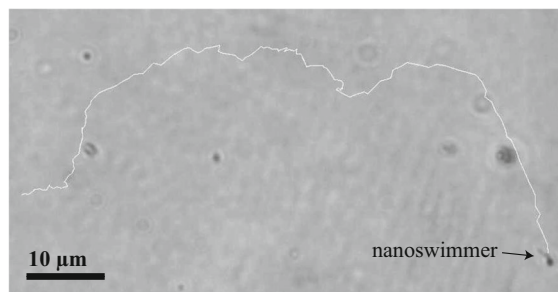
Fig. 4 Trajectory of a nanoswimmer. Brownian motion plays an influential role in the nano regime resulting in a jerky trajectory (see supplementary movie)
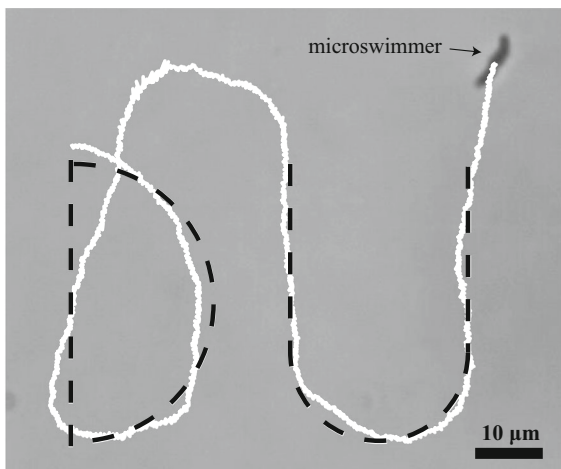
Fig. 5 Trajectory of a microswimmer. Using manual control, the microswimmer was manipulated to swim in a pattern that spells out DU (see supplementary movie)

$$\text{MSD} = \left\langle (\mathbf{r}(t) - \mathbf{r}(0))^2 \right\rangle, \qquad (7)$$

where $\mathbf{r}$ is the position at time t. Figure 6 shows the MSD as a function of τ for both micro- and nanoswimmers. The two-dimensional diffusion coefficient D is expressed as

$$D = \frac{1}{4} \lim_{t \to \infty} \frac{\mathrm{d}}{\mathrm{d}t} \text{MSD}. \qquad (8)$$

The diffusion coefficient for micro- and nanoswimmers are 0.1178 and 0.3670 μm^2/s respectively, which matched favorable with the theoretical values computed from Eq. (3).

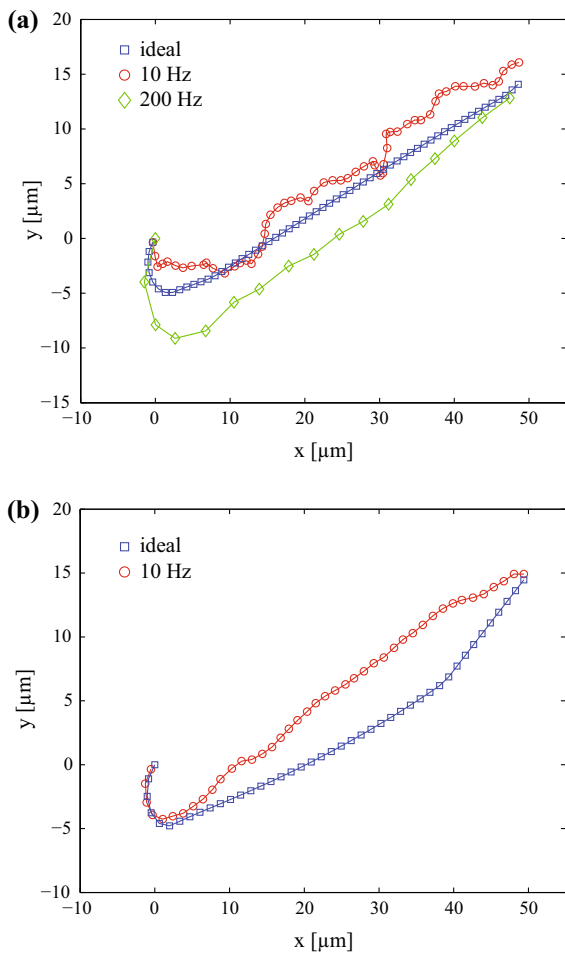Simulation of trajectories under Brownian disturbances

Using Eq. (5), we performed a simulation to map trajectories of the micro- and nanoswimmers (Fig. 7). The simulation demonstrates the feasibility to use real-time feedback control in the presence of Brownian motion as random disturbance, as shown in Eq. (6). The magnetic swimmer is omnidirectional, but for the purpose of demonstration in this simulation, we define a constraint for the maximum turning rate $\dot{\phi}$ as 0.2618 rad/s in order to simulate trajectories with curvatures. This way, we can observe the performance of the swimmers while moving in a straight path and turning. We set the initial heading angle as 225°, the initial position at (0, 0), and the
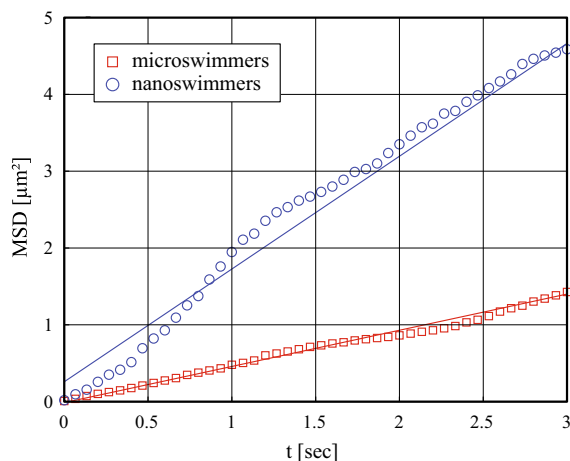
Fig. 6 Mean squared displacement (MSD) plotted for both microswimmers (*squares*) and nanoswimmers (*circles*) while the magnetic field is turned off

desired position at (50, 15). The average velocities for both the micro- and nanoswimmer were based on data fitting of velocities against frequency. The upper plot in Fig. 7 shows three simulated trajectories for a nanoswimmer: ideal swimming with no Brownian motion, swimming at 0.49 μm/s under 10 Hz rotation with Brownian motion at $D = 0.2841$ μm^2/s, and swimming at 9.8 μm/s under 200 Hz rotation with the same strength of Brownian motion. The bottom plot in Fig. 7 shows two simulations for microswimmers: ideal with no Brownian motion and swimming at 0.49 μm/s under 10 Hz rotation with Brownian motion at $D = 0.0944$ μm^2/s. The diffusion coefficients D are taking from the theoretical values calculated in a previous section. The simulations illustrate the influence of Brownian motion on the relative size and velocities of swimmers, which is evidenced with the smooth trajectory of the bigger and faster microswimmer while the nanoswimmer at 10 Hz have a jerky trajectory. In fact, the motion of the microswimmer with Brownian motion compares favorably with the ideal case. The increased velocity of the nanoswimmer at 200 Hz yields a much smoother trajectory, indicating the potential to overcome Brownian disturbance at nanoscale. However, as the scale of the swimmer decreases further, the effects of Brownian motion may entirely overwhelm the ballistic velocity of the nanoswimmers. A similar study on helical swimmers (Ghosh et al. 2013b), with the same order of magnitude in length scale as our nanoswimmers, also

Fig. 7 Simulation of trajectories of micro- and nanoswimmer. **a** Simulation of a nanoswimmer rotating at 10 Hz with no Brownian motion (*blue squares*), rotating at 10 Hz with Brownian motion (*red circles*), and rotating at 200 Hz with Brownian motion (*green diamonds*). **b** Simulation of a microswimmer rotating at 10 Hz with no Brownian motion (*blue squares*), rotating at 10 Hz with Brownian motion (*red circles*). (Color figure online)

suggests that the limitation in the smallest size for nanoswimmers is limited by thermal fluctuation, which corroborate well with our results and further validate the existence of a limitation on how small nanoswimmers can be.

Conclusion

In summary, we have demonstrated fabrication of micro- and nanoswimmers using magnetic self-assembly of MNPs. The chains and chain bundles constitute as

nanoswimmers and microswimmers, respectively. The use of MNPs offer scalability of swimmers' sizes by controlling magnetic aggregation. We have developed a magnetic control system to steer the magnetic swimmers in any direction in 2D. Two representative cases were shown to demonstrate steering of nanoswimmers and microswimmers in bulk fluid. In the case of nanoswimmers, the trajectories were strongly influenced by Brownian motion, resulting in a jerky trajectory, much like the trajectory from the experiment in Fig. 4. For microswimmers the motion is not influenced significantly by Brownian motion and was able to produce relatively smooth trajectories. We have investigated the diffusivity for both sizes of swimmer analytically and experimentally. Given the small velocity of the nanoswimmer at 10 Hz rotation, the Brownian noise was disruptive but does not overwhelm active propulsion. The simulated trajectory for nanoswimmer rotating at 200 Hz has shown that Brownian noise at nanoscale can be tolerated, therefore, does not break the paradigm of nanorobotics for drug delivery. The use of nanoparticles to assemble into controllable swimmers can enhance the ability for active manipulation for targeting in nanoparticulate drug delivery systems.

With the basic concept to fabricate controllable microswimmers from nanoparticle self-assembly, we hope to combine the robotic principles with advances of particulate drug delivery system. We will explore how these MNP swimmers may fit into circulation in the blood stream, extravasation through leaky vasculatures, and moving within the tumor microenvironment. Proof of concept experiment may be conducted using MEMS technology to evaluate whether the MNP swimmers may address some of the issue for the drug delivery paradigm.

References

Abbott J, Peyer K, Lagomarsino M, Zhang L, Dong L, Kaliakatsos I, Nelson B (2009) How should microrobots swim? Int J Robot Res 28:1434–1447

Avron JE, Kenneth O, Oaknin DH (2005) Pushmepullyou: an efficient micro-swimmer. New J Phys 7:234

Bae YH, Park K (2011) Targeted drug delivery to tumors: myths, reality and possibility. J Controll Release 153:198–205

Bajpai I, Balani K, Basu B (2013) Spark plasma sintered HA-Fe_3O_4-based multifunctional magnetic biocomposites. J Am Ceram Soc 96:2100–2108. doi:10.1111/jace.12386

Basarkar A, Singh J (2007) Nanoparticulate systems for polynucleotide delivery. Int J Nanomed 2:353–360

Biswal SL, Gast AP (2004) Rotational dynamics of semiflexible paramagnetic particle chains. Phys Rev E 69:041406

Cēbers A, Javaitis I (2004) Dynamics of a flexible magnetic chain in a rotating magnetic field. Phys Rev E 69:021404

Cheang UK, Roy D, Lee JH, Kim MJ (2010) Fabrication and magnetic control of bacteria-inspired robotic microswimmers. Appl Phys Lett 97:213704. doi:10.1063/1.3518982

Cheang UK, Lee K, Julius AA, Kim MJ (2014a) Multiple-robot drug delivery strategy through coordinated teams of microswimmers. Appl Phys Lett 105:083705

Cheang UK, Meshkati F, Kim D, Kim MJ, Fu HC (2014b) Minimal geometric requirements for micropropulsion via magnetic rotation. Phys Rev E 90:033007

Cheong FC, Grier DG (2010) Rotational and translational diffusion of copper oxide nanorods measured with holographic video microscopy. Opt Express 18:6555–6562

Clearfield A (1996) Current opinion in solid state and materials science. Curr Sci 1:268

Dobson J (2006) Magnetic nanoparticles for drug delivery. Drug Dev Res 67:55–60

Dogangil G, Ergeneman O, Abbott JJ, Pané S, Hall H, Muntwyler S, Nelson BJ (2008) Toward targeted retinal drug delivery with wireless magnetic microrobots. In: IEEE international conference on intelligent robots and systems, Nice, pp 1921–1926

Dreyfus R, Baudry J, Roper ML, Fermigier M, Stone HA (2005) Microscopic artificial swimmers. Nature 437:862–865

Elimelech M, Jia X, Gregory J, Williams R (1998) Particle deposition and aggregation: measurement, modelling and simulation. Butterworth-Heinemann, Boston

Fang W-X, He Z-H, Xu X-Q, Mao Z-Q, Shen H (2007) Magnetic-field-induced chain-like assembly structures of Fe_3O_4 nanoparticles. Europhys Lett 77:68004

Ferreira A, Agnus J, Chaillet N, Breguet J-M (2004) A smart microrobot on chip: design, identification, and control. IEEE/ASME Trans Mechatron 9:508–519

Fusco S, Chatzipirpiridis G, Sivaraman KM, Ergeneman O, Nelson BJ, Pané S (2013a) Chitosan electrodeposition for microrobotic drug delivery. Adv Healthc Mater 2:1037–1044

Fusco S, Chatzipirpiridis G, Sivaraman KM, Ergeneman O, Nelson BJ, Pané S (2013b) Chitosan electrodeposition for microrobotic drug delivery. Adv Healthcare Mater 2:1037–1044

Gao W et al (2012) Cargo-Towing fuel-free magnetic nanoswimmers for targeted drug delivery. Small 8:460–467. doi:10.1002/smll.201101909

Gao W, D'Agostino M, Garcia-Gradilla V, Orozco J, Wang J (2013) Multi-fuel driven Janus micromotors. Small 9:467–471

Gauger E, Stark H (2006) Numerical study of a microscopic artificial swimmer. Phys Rev E 74:021907

Gelperina S, Kisich K, Iseman MD, Heifets L (2005) The potential advantages of nanoparticle drug delivery systems in chemotherapy of tuberculosis. Am J Respir Crit Care Med 172:1487–1490

Ghosh A, Fischer P (2009) Controlled propulsion of artificial magnetic nanostructured propellers. Nano Lett 9:2243–2245. doi:10.1021/nl900186w

Ghosh A, Paria D, Singh HJ, Venugopalan PL, Ghosh A (2012) Dynamical configurations and bistability of helical nanostructures under external torque. Phys Rev E 86:031401

Ghosh A, Mandal P, Karmakar S, Ghosh A (2013a) Analytical theory and stability analysis of an elongated nanoscale object under external torque. Phys Chem Chem Phys 15:10817–10823

Ghosh A, Paria D, Rangarajan G, Ghosh A (2013b) Velocity fluctuations in helical propulsion: how small can a propeller Be. J Phys Chem Lett 5:62–68

Grady M, Howard M III, Molloy J, Ritter R, Quate E, Gillies G (1990) Nonlinear magnetic stereotaxis: three-dimensional, in vivo remote magnetic manipulation of a small object in canine brain. Med Phys 17:405–415

Kim DH, Cheang UK, Kohidai L, Byun D, Kim MJ (2010) Artificial magnetotactic motion control of Tetrahymena pyriformis using ferromagnetic nanoparticles: a tool for fabrication of microbiorobots. Appl Phys Lett 97:173702

Kim S et al (2013a) Fabrication and characterization of magnetic microrobots for three-dimensional cell culture and targeted transportation. Adv Mater. doi:10.1002/adma.201300223

Kim S et al (2013b) Fabrication and characterization of magnetic microrobots for three-dimensional cell culture and targeted transportation. Adv Mater 25:5863–5868

Leoni M, Kotar J, Bassetti B, Cicuta P, Lagomarsino MC (2009) A basic swimmer at low Reynolds number. Soft Matter 5:472–476

Liu X, Kim K, Zhang Y, Sun Y (2009) Nanonewton force sensing and control in microrobotic cell manipulation. Int J Robot Res 28:1065–1076

Magdanz V, Sanchez S, Schmidt OG (2013) Development of a sperm-flagella driven micro-bio-robot. Adv Mater 25:6588–6591

Manesh KM, Cardona M, Yuan R, Clark M, Kagan D, Balasubramanian S, Wang J (2010) Template-assisted fabrication of salt-independent catalytic tubular microengines. ACS Nano 4:1799–1804

Martel S et al (2007) Automatic navigation of an untethered device in the artery of a living animal using a conventional clinical magnetic resonance imaging system. Appl Phys Lett 90:114105

Mathieu J-B, Beaudoin G, Martel S (2006) Method of propulsion of a ferromagnetic core in the cardiovascular system through magnetic gradients generated by an MRI system. IEEE Trans Biomed Eng 53:292–299

Mody VV, Cox A, Shah S, Singh A, Bevins W, Parihar H (2014) Magnetic nanoparticle drug delivery systems for targeting tumor. Appl Nanosci 4:385–392

Mori N, Kuribayashi K, Takeuchi S (2010) Artificial flagellates: analysis of advancing motions of biflagellate micro-objects. Appl Phys Lett 96:083701. doi:10.1063/1.3327522

Najafi A, Golestanian R (2004) Simple swimmer at low Reynolds number: three linked spheres. Phys Rev E 69:062901

Ogrin FY, Petrov PG, Winlove CP (2008) Ferromagnetic microswimmers. Phys Rev Lett 100:218102

Ortega A, de la Torre JG (2003) Hydrodynamic properties of rodlike and disklike particles in dilute solution. J Chem Phys 119:9914–9919

Peyer KE, Zhang L, Nelson BJ (2011) Localized non-contact manipulation using artificial bacterial flagella Appl Phys Lett 99:174101 doi:10.1063/1.3655904

Purcell EM (1977) Life at low Reynolds number. Am J Phys 45:3–11

Singh R, Lillard JW Jr (2009) Nanoparticle-based targeted drug delivery. Exp Mol Pathol 86:215–223

Solovev AA, Mei Y, Bermúdez Ureña E, Huang E, Schmidt OG (2009) Catalytic microtubular jet engines self-propelled by accumulated gas bubbles. Small 5:1688–1692

Solovev AA, Xi W, Gracias DH, Harazim SM, Deneke C, Sanchez S, Schmidt OG (2012) Self-propelled nanotools. ACS Nano 6:1751–1756

Steager EB, Sakar MS, Kumar V, Pappas GJ, Kim MJ (2011) Electrokinetic and optical control of bacterial microrobots. J Micromech Microeng 21:035001

Sun C, Lee JS, Zhang M (2008) Magnetic nanoparticles in MR imaging and drug delivery. Adv Drug Delivery Rev 60:1252–1265

Tabak AF, Temel FZ, Yesilyurt S (2011) Comparison on experimental and numerical results for helical swimmers inside channels. In: IEEE/RSJ international conference on intelligent robots and systems (IROS), pp 463–468

Tan ML, Choong PF, Dass CR (2010) Recent developments in liposomes, microparticles and nanoparticles for protein and peptide drug delivery. Peptides 31:184–193

Temel FZ, Yesilyurt S (2011) Magnetically actuated micro swimming of bio-inspired robots in mini channels. In: International conference on mechatronics, Istanbul, pp 342-347. 13–15 April 2011

Tottori S, Zhang L, Qiu F, Krawczyk KK, Franco-Obregón A, Nelson BJ (2012) Magnetic helical micromachines: fabrication, controlled swimming, and cargo transport. Adv Mater 24:811–816. doi:10.1002/adma.201103818

Vach PJ et al (2013) Selecting for function: solution synthesis of magnetic nanopropellers. Nano Lett 13:5373–5378. doi:10.1021/nl402897x

Vartholomeos P, Fruchard M, Ferreira A, Mavroidis C (2011) MRI-guided nanorobotic systems for therapeutic and diagnostic applications. Annu Rev Biomed Eng 13:157–184

Venugopalan PL, Sai R, Chandorkar Y, Basu B, Shivashankar S, Ghosh A (2014) Conformal cytocompatible ferrite coatings facilitate the realization of a nanovoyager in human blood. Nano Lett 14:1968–1975. doi:10.1021/nl404815q

Vuppu AK, Garcia AA, Hayes MA (2003) Video microscopy of dynamically aggregated paramagnetic particle chains in an applied rotating magnetic field. Langmuir 19:8646–8653. doi:10.1021/la034195a

Xi W, Solovev AA, Ananth AN, Gracias DH, Sanchez S, Schmidt OG (2013) Rolled-up magnetic microdrillers: towards remotely controlled minimally invasive surgery. Nanoscale 5:1294–1297

Yesin KB, Exner P, Vollmers K, Nelson BJ (2005) Design and control of in vivo magnetic microrobots Medical Image Computing and Computer-Assisted Intervention 3749:819–826

Ytreberg FM, McKay SR (2000) Calculated properties of field-induced aggregates in ferrofluids. Phys Rev E 61:4107

Zhang H, Hutmacher DW, Chollet F, Poo AN, Burdet E (2005) Microrobotics and MEMS-based fabrication techniques for scaffold-based tissue engineering. Macromol Biosci 5:477–489